https://doi.org/10.5194/egusphere-2026-1545
Preprint. Discussion started: 29 April 2026

Application of radar remote sensing for cyclone damage mapping in Bangladesh: A coherence-based approach

Shadmin Islam Prova[1,2], Md. Shahoriar Sarker[1*], Rosdania Islam[3], Ridad Ibne Mahfuz[1]

[1]Department of Disaster Science and Climate Resilience, University of Dhaka, Dhaka-1000, Bangladesh
[2]Institute of Disaster Management and Vulnerability Studies, University of Dhaka, Dhaka-1000, Bangladesh
[3]Institute of Modern Languages, University of Dhaka, Dhaka-1000, Bangladesh

Correspondence to: Md. Shahoriar Sarker, Lecturer, Department of Disaster Science and Climate Resilience, University of Dhaka, Dhaka-1000, Bangladesh; Email: shahoriarsarker@du.ac.bd; cell: +880 1728948776

Abstract. Rapid and reliable assessment of cyclone-induced damage remains a major challenge in coastal regions where cloud cover and accessibility limit conventional approaches. This study presents a coherence-based Synthetic Aperture Radar (SAR) framework for identifying as well as quantifying cyclone-induced surface changes in coastal districts in Bangladesh. Multi-temporal Sentinel-1 data were analyzed using interferometric coherence to capture spatial and temporal variations associated with five major cyclones: Amphan (2020), Sitrang (2022), Mocha (2023), Hamoon (2023), and Remal (2024). A time-series approach incorporating multiple pre-, during-, and post-event image pairs was implemented to distinguish cyclone-driven changes from natural surface variability and to improve detection reliability. The results reveal a consistent decline in coherence during cyclone events followed by gradual recovery. Spatial analysis indicates that areas of significant coherence loss correspond to zones affected by flooding, vegetation damage, and structural disruption. Estimated damage extents varied across cyclones, with Remal (2024) showing the largest affected area (~601 km²), followed by Mocha (~474 km²), Amphan (~288 km²), Sitrang (~122 km²), and Hamoon (~117 km²). Validation using field observations and secondary data yielded an overall classification accuracy of 94%, confirming the robustness of the coherence-based approach. Complementary inundation mapping further demonstrated that coherence captures a broader spectrum of cyclone impacts beyond flood extent alone, including wind-induced damage and geomorphic changes. This study establishes multi-temporal SAR coherence analysis as a scalable, cloud-independent, and operationally effective tool for rapid post-cyclone damage assessment. The proposed framework enhances the reliability of disaster monitoring in complex coastal environments and offers strong potential for integration into near-real-time disaster response systems. Future research should focus on integrating multi-sensor datasets and long-term coherence time series to further refine damage characterization and reduce uncertainty.

1 Introduction

Tropical cyclones are one of the largest geophysical causes of loss of life and property, causing significant loss of life and widespread economic damage worldwide (Emanuel, 1987). Bangladesh, located along the northern coast of the Bay of Bengal, is particularly vulnerable due to its low-lying topography, dense population, and frequent cyclone landfalls. Over the past

https://doi.org/10.5194/egusphere-2026-1545
Preprint. Discussion started: 29 April 2026

decade, Bangladesh has experienced two of the most devastating cyclones in history (Islam & Peterson, 2009), while on average about four tropical cyclones and one flood-season event occur each year (Saha & Khan, 2014). In 2021, climate-related disasters led to economic losses estimated at USD 11.3 billion, accounting for approximately 2.47% of the country's GDP (WMO, 2022; National Adaptation Plan of Bangladesh (2023-2050), 2022). Rapid, reliable, and near-real-time damage assessment that delivers continuous information is essential for effective disaster monitoring, emergency response, and long-term resilience planning (Al Shafian & Hu, 2024).

Remote sensing data enables rapid post-disaster information acquisition, helping to understand spatial phenomena and providing authorities and scientists with objective data for informed decision-making (Ge et al., 2019; Washaya & Balz, 2018). Conventional post cyclone damage assessment methods such as optical satellite imagery and ground-based surveys are often hampered by cloud cover, adverse weather, and logistical constraints. Previous cyclone damage assessments have relied predominantly on optical satellite imagery (Landsat, Sentinel-2), sometimes supplemented with multi-sensor data for land-use and land-cover (LULC) analysis (Tazneen et al., 2021; Salman et al., 2024). The integration of GIS with remote sensing supports land-use-based damage interpretation, although persistent challenges remain in field validation, classification uncertainty, and the need for timely updates to hazard maps (Uddin & Matin, 2021).

Optical imagery, especially near nadir, often fails to detect wall damage in buildings with intact roofs, as it mainly captures roof condition and nearby debris rather than wall status. Synthetic Aperture Radar (SAR) provides a powerful alternative as it operates independently of weather and lighting conditions; Its ability to penetrate cloud cover and acquire data continuously makes it particularly suitable for monitoring cyclone-affected regions (Olen & Bookhagen, 2018;Bürgmann et al., 2000). The advantage of SAR is the use of the phase difference at SAR interferometric analysis. SAR particularly interferometric phase, can reveal damage in seemingly intact buildings, though visibility is strongly affected by side-looking geometry, layover, and shadowing (Plank, 2014).

Among SAR-based techniques, Interferometric SAR (InSAR) coherence, or the correlation between two images analysis has emerged as an effective approach for detecting surface changes by measuring the similarity between radar signals acquired through phase variation at different times (Touzi et al., 1999; Bürgmann et al., 2000) . It can be particularly beneficial for evaluating natural hazards linked to heavy precipitation such as cyclones, cyclone induced floods, seasonal or rain induced floods where continuous cloud cover can significantly limit the effectiveness of optical satellite imagery. (Tralli et al., 2005). Changes in land surface properties such as vegetation disturbance, structural damage, or flooding led to a reduction in coherence, allowing for spatial identification of affected areas. Previous studies have applied SAR-based change detection using different approaches, including intensity-based, coherence-based, and integrated multi-sensor methods (Ge et al., 2020). While optical datasets such as Landsat and Sentinel-2 remain widely used for large-scale damage assessment, their

https://doi.org/10.5194/egusphere-2026-1545
Preprint. Discussion started: 29 April 2026

effectiveness is limited in cyclone-prone regions due to persistent cloud cover and revisit constraints (Tazneen et al., 2021; Salman et al., 2024). Similarly, traditional single-pair coherence analyses often fail to account for natural temporal variability, making it difficult to distinguish cyclone-induced changes from seasonal or environmental fluctuations (Olen & Bookhagen, 2018).

The availability of Sentinel-1 SAR data has significantly improved the potential for operational damage assessment. With its C-band radar, near-global coverage, and short revisit interval, Sentinel-1 enables the construction of multi-temporal coherence time series for continuous monitoring (Torres et al., 2012). By analyzing coherence variations over time, it becomes possible to characterize baseline surface conditions and identify statistically significant deviations associated with extreme events. This multi-temporal approach reduces false detections and enhances the reliability of change identification, particularly in dynamic coastal environments. Despite these advancements, several challenges remain. Coherence measurements are influenced by factors such as vegetation dynamics, soil moisture variability, and imaging geometry, which can introduce noise into the signal. Moreover, heterogeneous land cover and rapid environmental changes in coastal regions complicate the interpretation of SAR-based results. Many existing methodologies also lack standardized frameworks that can be consistently applied across different cyclone events and geographic settings.

This study addresses these challenges by applying a multi-temporal coherence-based change detection approach to assess cyclone-induced damage in the most affected coastal Bangladesh. The analysis focuses on five major cyclones – Amphan (2020), Sitrang (2022), Mocha (2023), Hamoon (2023), and Remal (2024) and examines spatial patterns of coherence loss across the most affected districts, including Khulna, Satkhira, Barguna, Patuakhali, Bhola, Cox's Bazar, and Chattogram. By integrating multi-temporal SAR coherence analysis with secondary impact data, the study provides a consistent and scalable framework for mapping cyclone-induced surface changes. The findings aim to improve understanding of coherence behavior in complex deltaic environments and contribute to more effective disaster assessment and resilience planning in Bangladesh.

2 Study Area

The study focuses on coastal Bangladesh, one of the world's most cyclone-exposed deltaic regions, to evaluate SAR coherence change across major recent cyclones. Five cyclone events from 2019 – 2025 were selected for analysis which are Amphan (2020), Sitrang (2022), Mocha (2023), Hamoon (2023), and Remal (2024) based on verified impact reports from BMD, DDM, UNOSAT, and Copernicus. The most affected districts Khulna, Satkhira, Barguna, Patuakhali, Bhola, Cox's Bazar, and Chattogram were mapped to define the spatial extent for coherence evaluation.

https://doi.org/10.5194/egusphere-2026-1545
Preprint. Discussion started: 29 April 2026

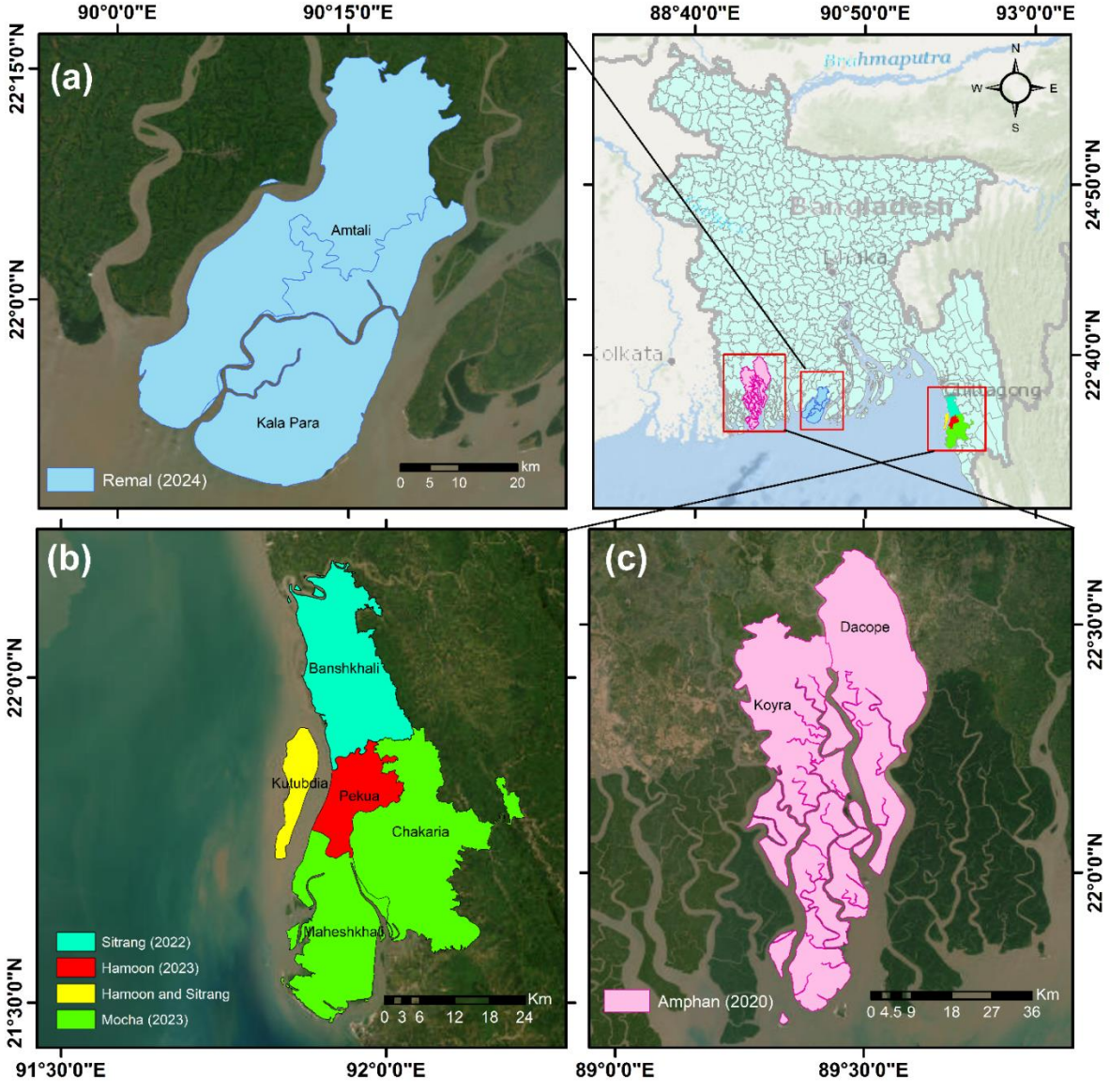

Figure 1 Study area location based on the cyclone landfall. (a) Areas affected by Cyclone Remal (2024); (b) Areas affected by Cyclone Hamoon (2023); Cyclone Mocha (2023), Cyclone Sitrang (2022); (c) Areas affected by Cyclone Amphan (2020). Base maps are from ESRI World Imagery and World Topographic Map, with data sources including Esri, Maxar, Earthstar Geographics, HERE, Garmin, OpenStreetMap contributors, and the GIS User Community | Powered by Esri.

These areas consistently experience severe wind, surge, and flooding impacts, making them suitable as our study area. Within these districts, selected upazilas represent the dominant coastal landscape such as low-lying tidal floodplains (Kalapara, Dacope, Koyra), exposed offshore islands (Kutubdia), and complex peri-urban coastal zones (Pekua, Maheshkhali, Chakaria). These settings share three features central to the analysis: (a) persistent inundation; (b) heterogeneous land cover; and (c) rapid

https://doi.org/10.5194/egusphere-2026-1545
Preprint. Discussion started: 29 April 2026

surface modification during cyclones. By incorporating multiple landfall locations from five cyclone events, the study area supports a comparative assessment of how multi-temporal SAR coherence captures spatial variability in cyclone impacts.

3 Methodology

3.1. InSAR Coherence Measurements

SAR systems are active microwave radars that measure both signal amplitude (return strength) and phase (wave offset) from reflected Earth surface waves. Each SAR image pixel is a complex value represented by real and imaginary parts that represent amplitude and phase, respectively. To compare two SAR images and compute coherence, they must be precisely aligned, with the secondary image typically resampled to match the primary one. Correlation and coherence are often used interchangeably, and coherence can be used to estimate phase noise (Mohammad, 2016). The correlationbetween two signals, S_1 and S_2, observed at interferometer apertures 1 and 2, is defined as:

$$Coherence = \frac{\langle S_1 S_2^* \rangle}{\sqrt{(\langle S_1 S_1^* \rangle \langle S_2 S_2^* \rangle}} \quad (1)$$

where S_1 and S_2 are the complex pixel values at times t = 1 and t = 2; s* is the complex conjugate of s; and ⟨ ⟩ represents the ensemble average. (Touzi et al., 1999; Zebker et al., 1992). Coherence is a normalized measure ranging from 0 to 1, with higher values indicating stable surfaces and lower values reflecting changes in phase or amplitude. For example, changes in surface elevation (like building damage), backscatter properties (such as vegetation growth or removal), or surface dielectric characteristics (like wet vs dry soil) can reduce coherence (Zebker et al., 1992). Thus, coherence provides a spatial and temporal estimate of where and when changes occur (Olen & Bookhagen, 2018). The accuracy of phase measurements depends on interferometric coherence, which can be reduced by factors like receiver noise, temporal changes in the scene, geometric baseline, and volume effects. The overall coherence loss is determined by combining these individual contributions (Moreira et al., 2013).

https://doi.org/10.5194/egusphere-2026-1545
Preprint. Discussion started: 29 April 2026

In this study, we used Sentinel-1 SAR coherence for Change Detection (CCD) to assess cyclone impacts by taking advantage of SAR's all-weather imaging capability, which overcomes cloud cover limitations in optical imagery (Phiri et al., 2021). We analyzed eight SAR acquisitions: three pre-cyclone pairs to establish normal surface variability, one pair during the cyclone, and three post-cyclone pairs to measure changes caused by the event. Using multiple pre-event pairs improves statistical characterization of normal coherence and enables more reliable detection of anomalous coherence loss linked to cyclone damage. Coherence generation, multi-temporal stacking, and conditional change detection were conducted in the ESA open-source SNAP platform, with results validated against ground truth and comparative remote sensing data. Thus, this methodology combines quantitative coherence metrics with qualitative interpretation of surface changes and terrain effects, enhancing detection of cyclone-related disturbances and reducing false positives.

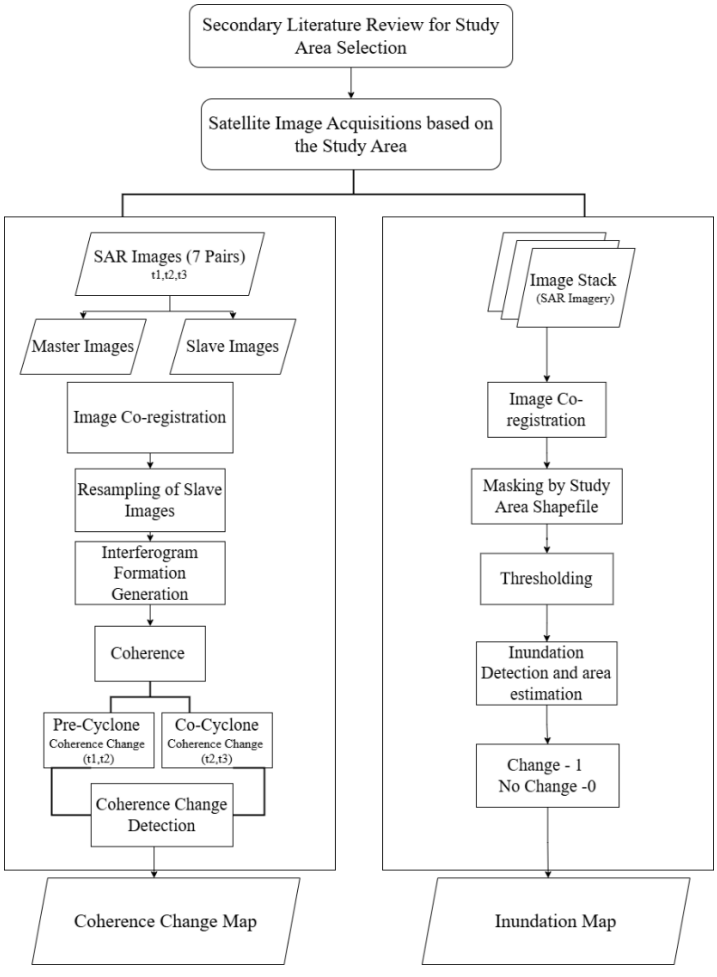

Figure 2 Methodological framework for this study shows conceptual and processing flowchart for conducting the research.

https://doi.org/10.5194/egusphere-2026-1545
Preprint. Discussion started: 29 April 2026

3.2 Data and Materials

This study used multi-temporal Sentinel-1 C-band Single Look Complex (SLC) SAR data acquired in Interferometric Wide Swath (IW) mode from Sentinel-1A's ascending orbit. VV-polarized C-band Interferometric Wide (IW) swath images were acquired from the Copernicus Sentinel-1 mission and analyzed with swath and burst selections adjusted to fully cover the cyclone-affected coastal districts. For each of the cyclones, a set of three pre-event (acquired at times t_1 and t_2) to establish a stable reference baseline, one during the event, and at least two post-event images acquired immediately after the cyclone at time t_3 to detect surface changes, generally consisting of three images before landfall and three after. Image pairs were selected to maintain short temporal baselines (typically ≤15 days) and acceptable perpendicular baselines (generally <100 m), ensuring phase stability for interferometric coherence estimation. The pre-event images acquired closest to the landfall date were selected as the master, and all other images were co-registered to this reference to generate a master–slave stack suitable for coherence computation. Coherent Change Detection (CCD) was applied using a normalized log-likelihood ratio test to identify statistically significant reductions in coherence. Thresholds were calibrated using a small sample dataset to minimize false positives and false negatives. The processed outputs were geocoded to generate spatially explicit change detections, including coordinates, change statistics, and temporal information. Final results were exported as structured datasets, enabling precise identification and analysis of cyclone-induced surface disturbances across the study area.

Table 1 The multi-temporal Sentinel-1 image pairs used for each cyclone demonstrate the systematic selection of the pre-, during-, and post-event acquisitions with controlled temporal and spatial baselines to ensure reliable coherence-based change detection.

Cyclone Name	Master	Slave	B⊥ (m)	Δt (days)
Remal (2024)	17 May 2024	30 March 2024	120	48
		23 April 2024	85	24
		05 May 2024	40	12
		29 May 2024	55	12
		10 June 2024	70	24
		22 June 2024	95	36
		04 July 2024	110	48
Hamoon (2023)	21 October 2023	15 September 2023	90	36
		27 September 2023	70	24
		09 October 2023	45	12

https://doi.org/10.5194/egusphere-2026-1545
Preprint. Discussion started: 29 April 2026

Cyclone Name	Master	Slave	B⊥ (m)	Δt (days)
		02 November 2023	55	12
		14 November 2023	80	24
		26 November 2023	100	36
		08 December 2023	120	48
Mocha (2023)	6 May 2023	31 March 2023	95	36
		12 April 2023	70	24
		24 April 2023	50	12
		18 May 2023	45	12
		30 May 2023	75	24
		11 June 2023	95	36
		23 June 2023	110	48
Sitrang (2022)	14 October 2022	8 September 2022	100	36
		20 September 2022	80	24
		02 October 2022	50	12
		26 October 2022	60	12
		07 November 2022	85	24
		19 November 2022	105	36
		01 December 2022	120	48
Amphan (2020)	19 May 2020	13 April 2020	90	36
		24 April 2020	70	25
		07 May 2020	45	12
		25 May 2020	50	6
		31 May 2020	75	12

https://doi.org/10.5194/egusphere-2026-1545
Preprint. Discussion started: 29 April 2026

Cyclone Name	Master	Slave	B⊥ (m)	Δt (days)
		11 June 2020	95	23
		24 June 2020	110	36

3.3 Coherence-based Damage Assessment

3.3.1 Pre-processing of SAR Imagery

To accurately detect cyclone-related damage and flooding, all Sentinel-1 Single Look Complex (SLC) images were processed using a consistent workflow in the Sentinel Application Platform (SNAP). The preprocessing began with organizing and stacking pre-, during-, and post-cyclone images to maintain temporal consistency and allow meaningful comparison over time. VV-polarized IW swath images were aligned through co-registration so that each pixel corresponded spatially across all images, minimizing errors caused by misalignment rather than actual surface change.

To improve image quality, multilooking was applied by averaging neighboring pixels in both range and azimuth directions, which helped reduce speckle noise and standardize pixel spacing. The data were resampled to a resolution of approximately 30 × 30 m and corrected for topographic effects using the SRTM 1-arcsecond (~30 m) Digital Elevation Model. Coherence was then calculated for consecutive image pairs across the time series to ensure the shortest possible temporal baseline, capturing subtle surface changes more effectively. These coherence values were combined into a multi-dimensional stack, where spatial dimensions (x, y) were linked with a temporal component, enabling pixel-wise analysis of coherence behavior over time. Resampling and terrain correction ensured that all images shared a consistent spatial reference and geometric accuracy. As a result, the final dataset was well-aligned, radiometrically consistent, and suitable for reliable coherence analysis. For each cyclone, coherence was computed for multiple pre- and post-event image pairs, generating several coherence layers that allowed clear separation of surface conditions before and after the event. This multi-temporal structure reduced phase noise, improved baseline characterization, and enhanced sensitivity to cyclone-induced changes. The processed coherence maps were terrain-corrected and exported in GeoTIFF format for further spatial analysis.

3.3.2 Damage Mapping

After preprocessing, interferometric coherence was calculated for each image pair to represent the degree of similarity between acquisition times. These coherence layers were then combined into a multi-temporal stack, enabling direct comparison between normal surface conditions and those affected by the cyclone. Damage detection was carried out by identifying pixels that showed significant reductions in coherence compared to the pre-event baseline. Such decorrelation typically indicates surface disturbances such as flooding, vegetation damage, or structural destruction. Conditional expressions were applied to classify these changes, allowing the extraction of affected areas across the study region. To improve the robustness of the results,

https://doi.org/10.5194/egusphere-2026-1545
Preprint. Discussion started: 29 April 2026

sensitivity analyses were performed by adjusting coherence thresholds and evaluating how small variations influenced the mapped damage extent. Different threshold values were applied to each SAR pair within SNAP to ensure that the detected changes accurately reflected the impact of each cyclone.

3.3.3 Post Processing

Multiple coherence layers, typically representing pre-, during-, and post-event stages, were stacked to support temporal comparison and improve the reliability of change detection. Damage areas were identified using band-math operations, where pixels showing significant decorrelation relative to baseline conditions were classified as affected. Threshold values were applied to distinguish between stable and disturbed areas, thus resulting in binary damage maps. These maps were then geocorrected, visualized, and exported for integration into GIS platforms such as ArcGIS. Optional post-processing, such as median filtering, was applied to reduce noise in the binary damage maps. The coherence-based damage layers were validated by cross-referencing with official cyclone reports and internal consistency checks comparing baseline pre-event coherence.

3.4 Inundation Mapping

To complement the SAR-based damage assessment, inundation mapping was conducted using Sentinel-1 VV-polarized GRD imagery in Google Earth Engine (GEE). This approach allowed spatially consistent identification of flood-affected areas during those cyclone events. For each event, two image composites were generated: one representing pre-flood conditions and another capturing the situation during the cyclone. Sentinel-1 data were filtered by acquisition mode, orbit, and polarization, then processed using median compositing to reduce noise and highlight persistent water signals. Flooded areas were identified through backscatter thresholding, while permanent water bodies were masked using pre-flood imagery to isolate newly inundated areas. The resulting difference between pre-flood and during-flood water masks produced a binary inundation layer, effectively capturing the spatial extent of cyclone-induced flooding. Flood extent maps were exported from GEE for integration with field validation and further spatial analysis.

3.5 Validation and Accuracy Assessment

Validation was essential to assess the accuracy of the coherence-based damage detection results. A field-based validation campaign was conducted for Cyclone Remal (2024), comparing satellite-derived changes with actual ground conditions within the Kala Para upazila and adjacent coastal areas. Representative validation points were selected from coherence maps using Google Earth Pro, covering both low-coherence (potentially damaged) and high-coherence (stable) areas. These points were georeferenced and visited in the field using GPS-enabled devices, where photographs and observations were collected to document surface conditions such as structural damage, vegetation loss, and flood impacts.

The field observations were then compared with the corresponding locations on the coherence maps to evaluate spatial accuracy and consistency. Any mismatches were analyzed to identify possible sources of error, including timing differences,

https://doi.org/10.5194/egusphere-2026-1545
Preprint. Discussion started: 29 April 2026

vegetation recovery, or mixed-pixel effects. For earlier cyclone events (e.g., Sitrang, Amphan, Mocha, Hamoon) where field validation was not possible, validation relied on secondary data sources, published reports, and comparisons with existing damage assessments. To quantify accuracy, predicted damage areas were compared with reference data using a confusion matrix and Kappa coefficient. This provided a systematic evaluation of classification performance, helping to assess the reliability of the coherence-based approach across different cyclone events.

4 Results

4.1 Summary of Coherence Change

The temporal behaviour of mean coherence values across the five major cyclonic events (Fig 4) shows a consistent V-shaped decline during the cyclone event, followed by gradual post-event recovery, reflecting the extent of surface disturbance. In this study context, low coherence indicates areas affected by flooding, structural damage, or vegetation disturbance, while high coherence corresponds to stable, undisturbed surfaces.

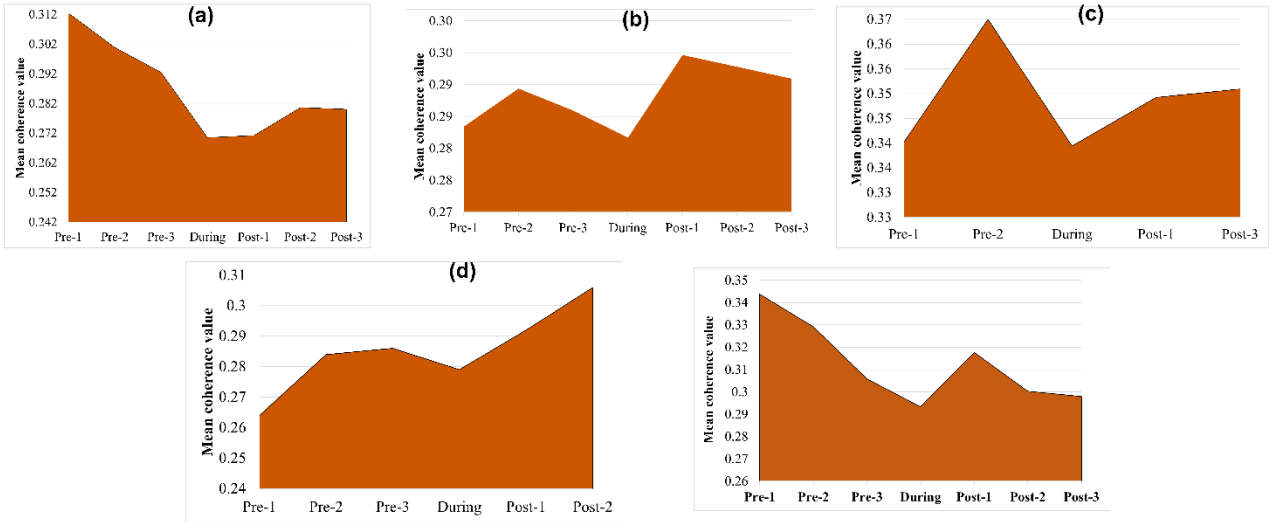

Figure 3 Mean Coherence Change graph of (a) Cyclone Remal (2024); (b) Cyclone Hamoon (2023); (c) Cyclone Mocha (2023); (d) Cyclone Sitrang (2022); (e) Cyclone Amphan (2020).

For Cyclone Remal (2024), the coherence value decreased from ~0.31 pre-event to ~0.27 during the event, rising to ~0.28 afterward. Cyclone Hamoon (2023) showed a similar shift from ~0.289 to ~0.275 before steady recovery. Cyclone Mocha (2023) presented the most pronounced drop, falling from ~0.37 to ~0.34. Cyclone Sitrang (2022) declined from ~0.28 to ~0.27 with a more prolonged recovery phase, while Cyclone Amphan (2020) decreased from ~0.34 to ~0.29 and stabilized near ~0.30 in later post-event scenes. These declines reflect widespread decorrelation driven by intense rainfall, canopy disturbance, inundation, and localized structural impacts, whereas post-event increases indicate restoration of surface scattering as water

https://doi.org/10.5194/egusphere-2026-1545
Preprint. Discussion started: 29 April 2026

receded and vegetation recovered. Although magnitudes varied, stronger cyclones such as Remal and Amphan produced deeper coherence drops, which signal higher levels of surface disruption. The consistent pattern across events demonstrates its capacity to capture both immediate disturbance and short-term recovery processes, and provides the quantitative foundation for the spatial damage mapping.

4.2 Coherence-Based Damage Maps

The coherence-based detection maps in Fig 5 illustrate the spatial distribution of cyclone-induced damage across those five cyclonic events. Each map presents areas of reduced coherence, representing probable surface or structural disturbance caused by the respective cyclone. In all events, zones categorized as “damage” (shown in yellow) correspond to areas where coherence dropped significantly between pre- and during-event SAR images, indicating sudden physical or environmental alterations.

https://doi.org/10.5194/egusphere-2026-1545
Preprint. Discussion started: 29 April 2026

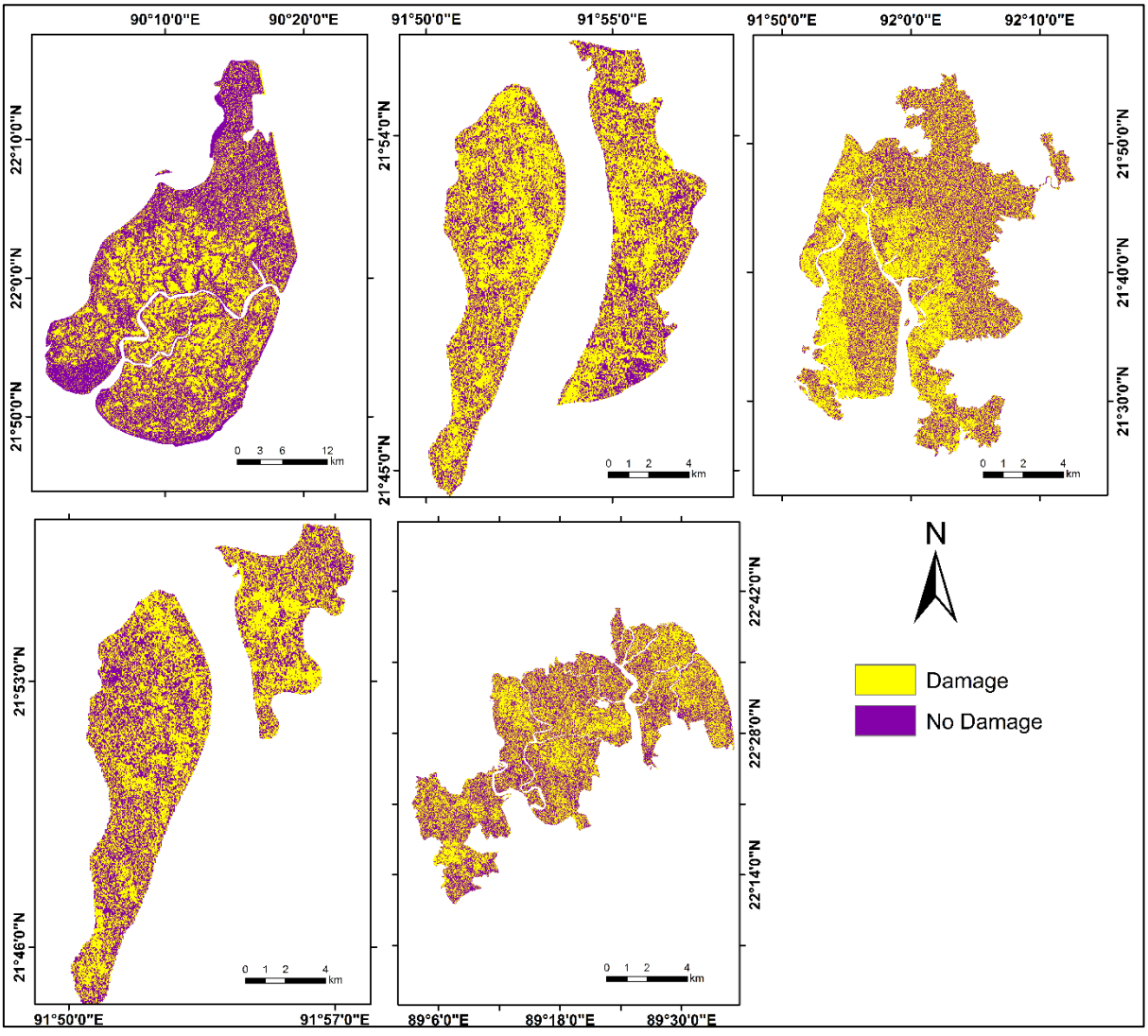

Figure 4 **Coherence-based** damage map of (a) Cyclone Remal (2024); (b) Cyclone Hamoon (2023); (c) Cyclone Mocha (2023); (d) Cyclone Sitrang (2022); (e) Cyclone Amphan (2020).

During Cyclone Remal (2024), the southern coastal upazilas - including Koyra, Paikgacha, and Dacope - exhibited extensive coherence loss. Approximately two-thirds of the region displayed reduced coherence values, particularly along riverine and low-lying zones. This spatial pattern suggests widespread inundation and vegetation disturbance, consistent with field reports of prolonged waterlogging and embankment breaches. For Cyclone Hamoon (2023), notable coherence reduction occurred in the western coastal belt of Cox's Bazar and the adjacent offshore island areas. High concentrations of damaged zones appeared near Kutubdia and Maheshkhali, aligning with the cyclone's landfall trajectory. The eastern portion showed relatively higher coherence retention, indicating localized but intense impacts rather than uniform damage across the area. Cyclone Mocha

https://doi.org/10.5194/egusphere-2026-1545
Preprint. Discussion started: 29 April 2026

(2023) reveals one of the most extensive spatial footprints of coherence loss among all studied events. Widespread yellow zones are visible across Teknaf, Ukhia, and Maheshkhali, reflecting severe disturbance to vegetation and built-up areas. Coastal exposure and storm surge likely contributed to the pronounced loss of phase stability. The similar distribution of low-coherence patches highlights the scale and intensity of Mocha's landfall in southern Cox's Bazar. In the case of Cyclone Sitrang (2022), coherence reduction was comparatively moderate but still concentrated along the western portion of Chattogram and the offshore islands. The inland regions retained higher coherence, suggesting partial shielding from storm surge and wind. The damage pattern here reflects a cyclone of moderate intensity whose impacts were geographically constrained. And finally, Cyclone Amphan (2020) demonstrates the most intense and spatially coherent pattern of damage, particularly across Satkhira and Khulna districts. Extensive coherence loss occurred along the coastal polders and agricultural belts, with localized patches of stability in higher elevation areas. The widespread loss of coherence aligns with the well-documented devastation caused by Amphan's strong winds and tidal surge. This consistent reduction in coherence across multiple events highlights our research method's sensitivity to structural and environmental disruption induced by tropical cyclones.

4.3 Inundation Scenario

The inundation maps of the study cyclones in Fig 6 show clear differences in the extent and spatial concentration of floodwater across the affected region. Cyclone Remal (2024) displays the most widespread inundation, with dense clusters of flooded pixels spreading across the southern and southwestern floodplains.

https://doi.org/10.5194/egusphere-2026-1545
Preprint. Discussion started: 29 April 2026

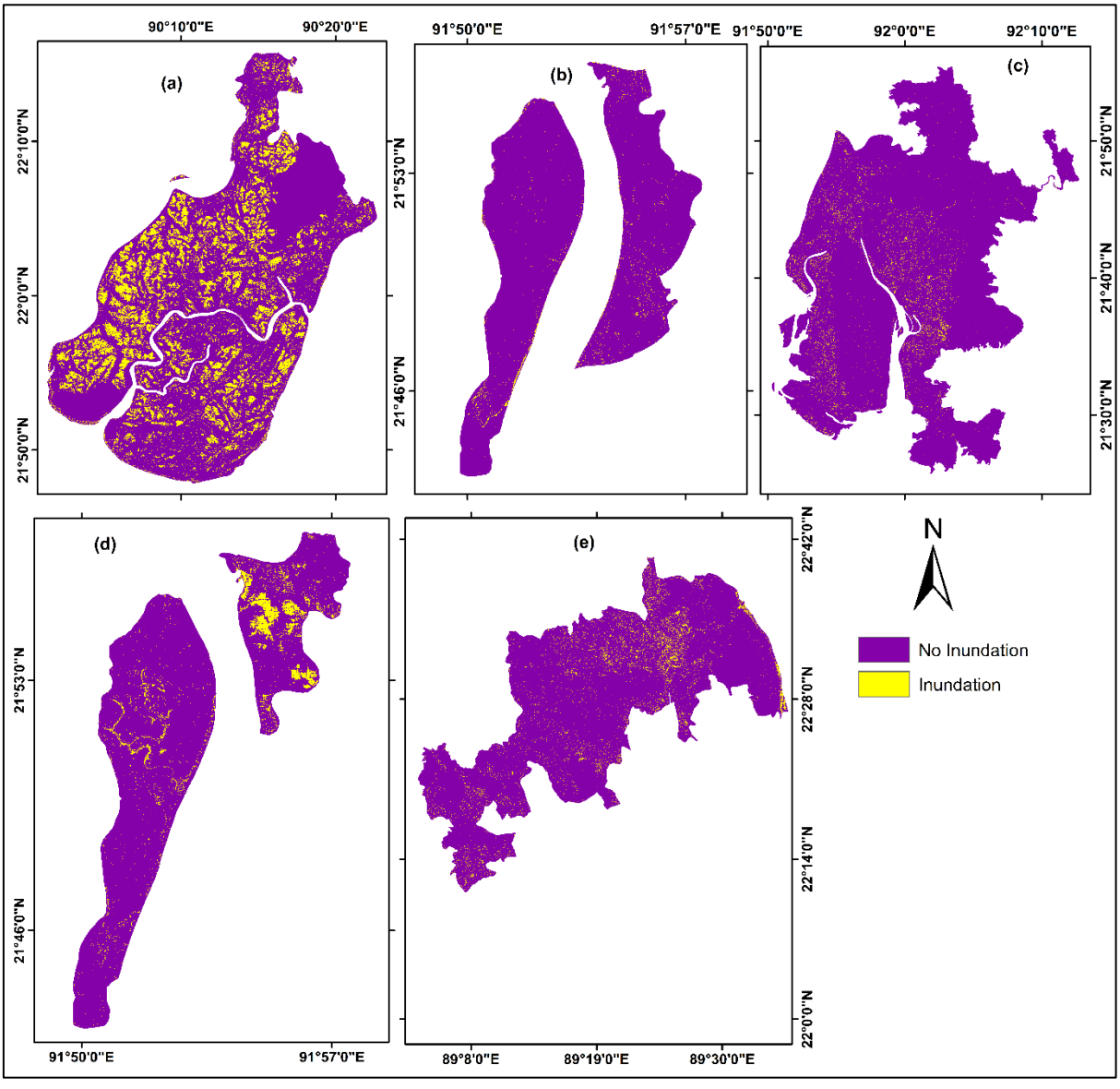

255 **Figure 5** Inundation Maps of (a) Cyclone Remal (2024); (b) Cyclone Hamoon (2023); (c) Cyclone Mocha (2023); (d) Cyclone Sitrang (2022); (e) Cyclone Amphan (2020).

On the other hand, Cyclone Hamoon (2023) shows a much narrower inundation footprint mainly along the coastal barrier islands. Most inland areas remain unaffected, indicating that the cyclone produced limited inland flooding despite notable wind impacts captured in coherence reduction. A similar pattern is visible for Cyclone Sitrang (2022), where inundation is visible
260 in the northern tip of the island, and the remaining zone shows no major flood presence. Cyclone Mocha (2023) presents a broader but relatively shallow inundation pattern around the Cox's Bazar region. Flooded pixels are scattered and

https://doi.org/10.5194/egusphere-2026-1545
Preprint. Discussion started: 29 April 2026

discontinuous, suggesting localized water accumulation rather than widespread surge. Cyclone Amphan (2020) comparatively shows a mixed scenario, with moderate inland inundation expanding across settlements and river-adjacent areas.

4.4 Result Validation

265 To validate the Sentinel-1 SAR-based coherence map for Cyclone Remal (2024), a total of 50 representative points were initially selected using the predicted damaged areas. These points were chosen to represent varying levels of predicted damage and corresponding coherence values. The selected points were successfully evaluated through field visits and visual confirmation, allowing direct comparison with the predicted damage map. Each point was categorized as True Positive (TP), False Positive (FP), True Negative (TN), or False Negative (FN) based on the agreement between ground observations and the
270 SAR-derived predictions.

https://doi.org/10.5194/egusphere-2026-1545
Preprint. Discussion started: 29 April 2026

Figure 6 Damages of Cyclone Remal (2024) found during field validation in Kala Para Subdistrict.

https://doi.org/10.5194/egusphere-2026-1545
Preprint. Discussion started: 29 April 2026

4.5 Damage Accuracy Assessment

Field validation after Cyclone Remal further substantiated mapping reliability. Among the fifty ground reference points, twenty-six out of twenty-seven damaged points were correctly identified with only one false negative despite a year-long gap, which indicates high classification accuracy. And of twenty-four undamaged points, twenty-one were correctly classified, with a little override. In total, 47 points out of 50 points were accurately mapped. This classification produced an overall 94% accuracy, indicating a strong relationship between SAR-derived results and field observations. The accuracy level aligns with established SAR-based disaster mapping performance, reinforcing the robustness of coherence-based assessment for rapid post-cyclone analysis.

4.6 Inundation Accuracy Assessment

Water body detection produced two classes: Inundated and Non-Inundated. The overall accuracy of classification is 94.12%, with a Kappa coefficient of 0.87. The producers' and users' accuracy for both classes is similar. 95.45% for Inundated and 91.67% for Non-Inundated classes (Table 2).

Table 2 Accuracy assessment result for the inundation mapping.

Class Name	Inundated	Non-Inundated	Producer's accuracy (%)	User's accuracy (%)
Inundated	42	2	95.45	95.45
Non-Inundated	2	22	91.67	91.67

5 Discussion

The results establish interferometric coherence as an effective and quantitatively dependable indicator of cyclone-induced surface change and disturbance. The observed temporal decline and gradual recovery after the landfall explain the short-term destabilization caused by cyclone winds, while the spatial distribution of coherence loss closely matches cyclone intensity from the secondary literature reviews. Partial overlap with inundation layers confirms that coherence captures flooding and inundation, wind-caused damage, and land surface changes within a single radar-derived measure. Thus, CCD as a method offers key advantages such as cloud independence, sensitivity to both flooded and wind-damaged surfaces, and scalability for temporal monitoring proved as a superior alternative to other optical or field-based damage monitoring and assessment methods.

https://doi.org/10.5194/egusphere-2026-1545
Preprint. Discussion started: 29 April 2026

5.1 Comparison of Cyclone Damage Scenario with Inundation Scenario

The coherence-based damage maps revealed clear variations in both the spatial extent and distribution of affected areas. The findings emphasized the sensitivity of the method to threshold selection as well as underlying cyclone dynamics. For instance, Cyclone Remal exhibited a broad low-coherence zone around Koyra and Dacope, aligning with reported inundation and embankment failures, while Hamoon showed a more localized footprint around Kutubdia, reflecting concentrated wind-energy dissipation. On the other hand, Mocha produced a widespread and relatively uniform pattern of decorrelation across southern Cox's Bazar, consistent with its extensive wind field. These spatial patterns demonstrate a strong link between cyclone characteristics and coherence response, allowing differentiation between varying levels of disturbance intensity. When compared with inundation maps, coherence-based results consistently captured a broader spectrum of impacts. In most cases, less than half of the low-coherence pixels overlapped with flooded areas, indicating that flooding alone does not account for the observed damage signals. Significant decorrelation was frequently detected in inland regions with little or no inundation, where field observations confirmed structural damage, vegetation loss, and surface disruption caused primarily by high winds. For example, during Remal, notable coherence loss was observed in Dhulasar and Nishanbaria unions despite limited water presence, while Hamoon produced strong inland damage signals in Barabakia and Lemshikhali. Similar patterns were evident for Mocha and Sitrang, where decorrelation was largely associated with wind-driven impacts rather than hydrological change, and Amphan showed both overlapping and distinct zones of flood-related and wind-induced damage. This combined analysis demonstrates that coherence loss reflects multiple interacting processes, including flooding, wind damage, and geomorphic disturbance, rather than a single hazard component. The integration of inundation mapping, spatial clustering, temporal coherence behavior, and field validation strengthens confidence in the results, confirming that coherence-based change detection provides a more comprehensive representation of cyclone impacts than flood mapping alone. Its ability to operate independently of cloud cover and daylight, while capturing both water-related and wind-induced changes, makes it particularly effective for rapid post-event assessment in data-constrained environments such as Bangladesh. Moreover, the observed coherence patterns are consistent with findings from other cyclone and hurricane studies, suggesting that the approach is both physically meaningful and transferable across different geographic and hazard contexts.

5.2 Contribution of this study considering current context

This study contributes socially by improving rapid, accurate assessment of cyclone-induced damage in Bangladesh's vulnerable coastal communities. The coherence-based framework offers disaster management agencies, ministries, and humanitarian actors a cost-effective, cloud-independent tool for identifying affected areas, planning rescue operations, and allocating resources efficiently. Integrating satellite data with ground validation enables operational assessment even in logistically challenging settings. The approach supports resilience building by informing mitigation strategies, infrastructure planning, and preparedness initiatives. Ultimately, it strengthens community safety, safeguards livelihoods, and enhances climate-adaptive capacity in cyclone-prone coastal regions.

https://doi.org/10.5194/egusphere-2026-1545
Preprint. Discussion started: 29 April 2026

5.3 Limitations

The study has a few limitations despite its strengths. The lack of socioeconomic and infrastructural data limited our first-hand contextual understanding of vulnerability and recovery processes in the cyclone-affected areas. The validation dataset derived from ground reference points was initially identified through visual interpretation of the raw imagery and subsequently crosschecked using area-specific secondary information of structural damage to improve reliability. Because of the temporal gap between the last recent cyclonic event, cyclone Remal and the field validation to reduce the limitation of direct, event-time ground data were unavailable. This may have introduced some uncertainty in the validated data, particularly for water-inundation-related impacts such as damage to croplands. Future research should integrate multi-sensor platforms SAR, optical, LiDAR, and hyperspectral, to overcome single-sensor constraints and enable more detailed 3D surface deformation mapping in terms of cyclones.

6 Conclusion & Recommendations

Effective disaster management strategies are critical for enabling rapid and comprehensive responses to cyclonic events, ultimately reducing their overall impacts. In hazard-prone regions, the development of a SAR coherence-based framework offers a practical means of identifying and mapping affected areas. Beyond post-event assessment, this approach also holds potential as a detection tool in remote or poorly monitored regions, where traditional observation systems may fail to capture the full extent of an event. The findings of this study highlight the importance of integrating robust remote sensing techniques into disaster monitoring systems. The application of Coherent Change Detection (CCD) proved effective for assessing cyclone-induced damage, demonstrating operational feasibility and accuracy. The observed findings from this study are consistent with findings from similar studies conducted in regions such as the United States, Japan, Italy, and Mozambique, reinforcing the broader applicability of this approach. The following conclusions can be drawn from the findings of this study:

1. The coherence maps consistently reveal substantial reductions in phase stability, thus reflecting structural deformation, vegetation disturbance, and inundation.
2. Temporal analysis shows a sharp decline in coherence within several days of landfall, followed by a gradual recovery as floodwaters receded and vegetation regenerated, indicating a deeper decorrelation between cyclone damage and coherence value loss.
3. Field validation confirmed strong alignment between the mapped disturbance and the real post-cyclone scenario. The overall accuracy of 94% demonstrates the reliability of CCD for post-cyclone assessment.
4. CCD has several advantages, such as all-weather independence, rapid data availability, and sensitivity to subtle structural or surface changes. With accurate co-registration and baseline selection, the false positives can be minimized.

https://doi.org/10.5194/egusphere-2026-1545
Preprint. Discussion started: 29 April 2026

Although this study focuses on coherence-based cyclone damage detection using C-band SAR data from the Sentinel-1 mission, future research could further enhance this methodology through long-term coherence time-series analysis. Approaches similar to those proposed by Olen & Bookhagen, 2018 could improve the identification of unusual surface changes while reducing uncertainties associated with seasonal variability. When combined with relevant local datasets, such as population distribution and infrastructure information, coherence-based damage mapping can provide valuable insights for identifying and prioritizing impacted regions following natural hazards. The study overall demonstrated an empirically validated relationship between coherence loss and cyclone-induced damage areas with a scalable and repeatable approach. To maximize national capacity, the Coherence Change Detection workflow can be integrated into a centralized GIS-based Disaster Data Management System or HCTT interactive dashboards to support D-Form reporting, Joint Needs Assessments, and PDNA processes within 48 to 72 hours after a cyclone landfall.

7 Appendices

Appendix A: Field Validation Images

(a)

(b)

https://doi.org/10.5194/egusphere-2026-1545
Preprint. Discussion started: 29 April 2026

(c)

(d)

(e)

(f)

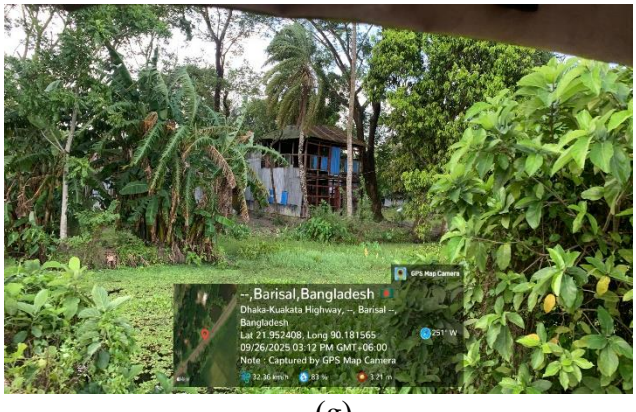

(g)

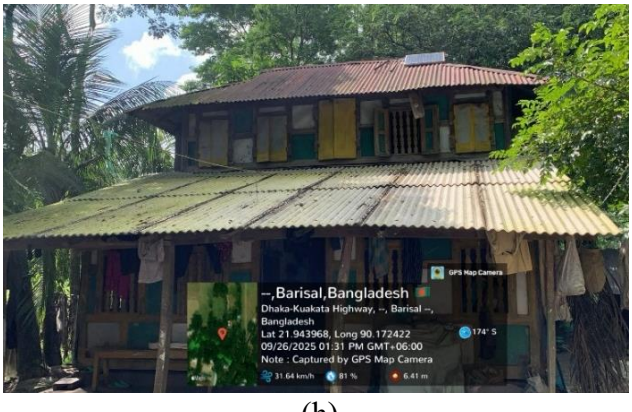

(h)

https://doi.org/10.5194/egusphere-2026-1545
Preprint. Discussion started: 29 April 2026

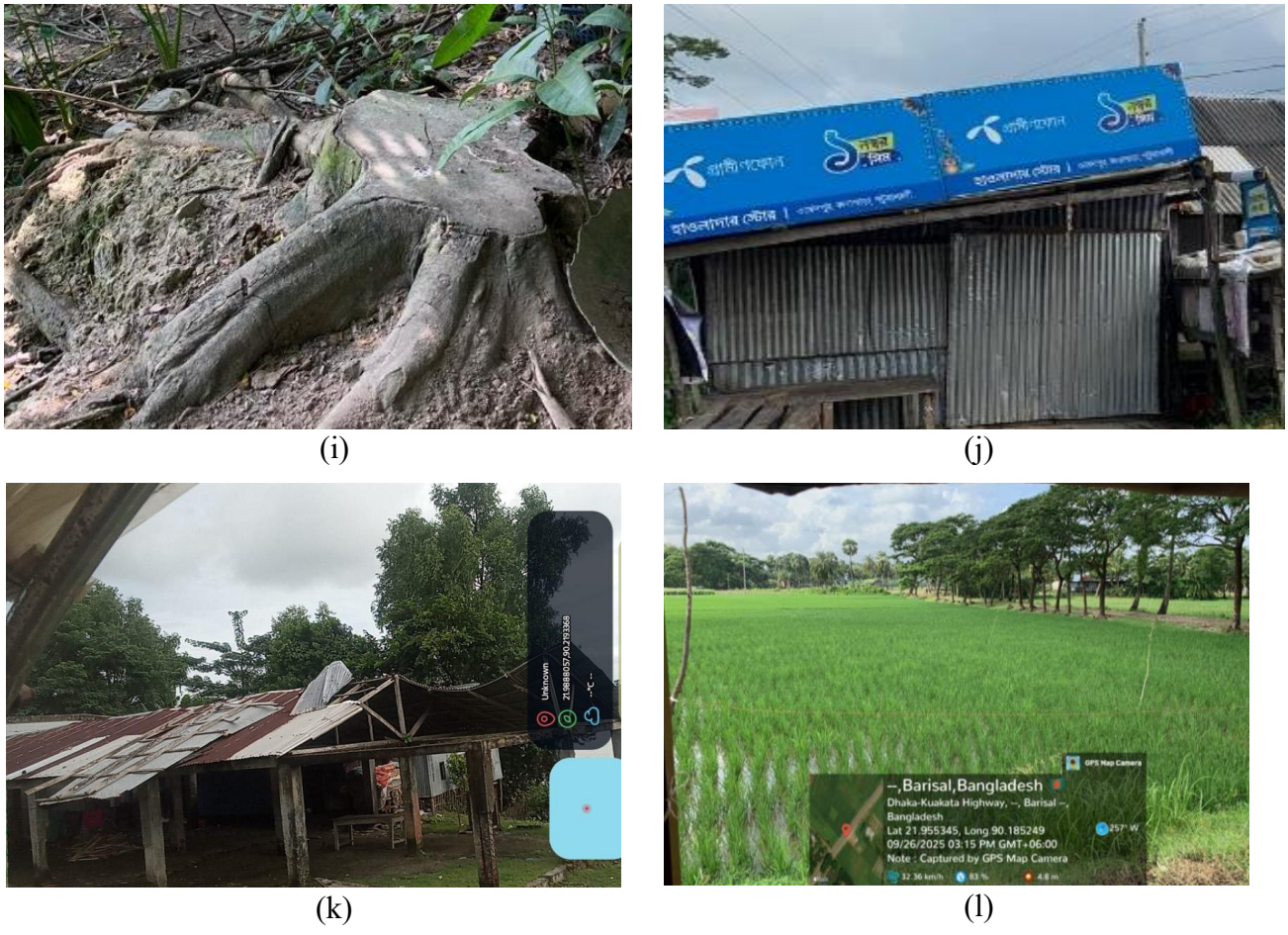

Figure A1 Field validation images taken in Kala Para subdistrict, Patuakhali for the damage validation of cyclone Remal.

Code, data, or code and data availability

Sentinel-1 GRD and SLC data used in this study are freely available from the Copernicus Open Access Hub (https://browser.dataspace.copernicus.eu/) and the ASF Vertex archive (https://search.asf.alaska.edu/). The SNAP software used for data processing is freely available. The code developed for this study has been made available via a Zenodo repository

https://doi.org/10.5194/egusphere-2026-1545
Preprint. Discussion started: 29 April 2026

(DOI: https://doi.org/10.5281/zenodo.19857126). The validation datasets supporting the findings of this study are available from the corresponding author upon reasonable request.

Author contributions

SIP carried out the conceptualization, acquired funding, investigation, data curation and validation, formal analysis of the data, visualization, and writing of the original draft of the manuscript. MSS contributed to conceptualization, supervision of the study, designing the methodology, writing, review and editing, and visualization. RI was involved in data curation, visualization, and writing of the original draft. RIM contributed to methodology, software, and result visualization. All authors were involved in reviewing and editing the manuscript.

Competing interests

The authors declare that they have no conflict of interest.

Disclaimer

The authors bear the ultimate responsibility for providing appropriate place names. Views expressed in the text are those of the authors and do not necessarily reflect the views of the publisher.

Acknowledgements

The authors express their sincere gratitude to the Department of Disaster Science and Climate Resilience at the University of Dhaka for providing the necessary research facilities to support this study. The authors also gratefully acknowledge the ESA Copernicus Data Space Ecosystem Open Access Hub for supplying the SAR imagery used in this study through their data portal (https://browser.dataspace.copernicus.eu/). A very small part of this research used artificial intelligence for grammar correction and to improve readability.

Financial support

This research has not received any funds.

https://doi.org/10.5194/egusphere-2026-1545
Preprint. Discussion started: 29 April 2026

Review statement

The review statement will be added by Copernicus Publications, listing the handling editor as well as all contributing referees according to their status, anonymous or identified.

References

Al Shafian, S., & Hu, D.: Integrating Machine Learning and Remote Sensing in Disaster Management: A Decadal Review of Post-Disaster Building Damage Assessment, Buildings, 14(8), Multidisciplinary Digital Publishing Institute (MDPI), https://doi.org/10.3390/buildings14082344, 2024.

Bürgmann, R., Rosen, P. A., & Fielding, E. J.: Synthetic Aperture Radar Interferometry to Measure Earth's Surface Topography and Its Deformation, Annu. Rev. Earth Planet. Sci., 28, https://doi.org/10.1146/annurev.earth.28.1.169, 2000.

Emanuel, K. A.: The dependence of hurricane intensity on climate, Nature, 326, 483–485, https://doi.org/10.1038/326483a0, 1987.

Ge, P., Gokon, H., Meguro, K., & Koshimura, S.: Study on the intensity and coherence information of high-resolution ALOS-2 SAR images for rapid massive landslide mapping at a pixel level, Remote Sensing, 11(23), https://doi.org/10.3390/rs11232808, 2019.

Mastro, P., Masiello, G., Serio, C., & Pepe, A.: Change Detection Techniques with Synthetic Aperture Radar Images: Experiments with Random Forests and Sentinel-1 Observations, Remote Sensing, 14(14), https://doi.org/10.3390/rs14143323, 2022.

Mohammad, D.: 3-D Surface Deformation Model from Sub-pixel Correlation of Optical Imagery and InSAR, (2016).

Moreira, A., Prats-Iraola, P., Younis, M., Krieger, G., Hajnsek, I., & Papathanassiou, K. P.: A tutorial on synthetic aperture radar, IEEE Geosci. Remote Sens. Mag., 1(1), 6–43, https://doi.org/10.1109/MGRS.2013.2248301, 2013.

National Adaptation Plan of Bangladesh (2023–2050), 2022.

Olen, S., & Bookhagen, B.: Mapping damage-affected areas after natural hazard events using Sentinel-1 coherence time series, Remote Sensing, 10(8), https://doi.org/10.3390/rs10081272, 2018.

Phiri, D., Simwanda, M., & Nyirenda, V.: Mapping the impacts of cyclone Idai in Mozambique using Sentinel-2 and OBIA approach, S. Afr. Geogr. J., 103(2), 237–258, https://doi.org/10.1080/03736245.2020.1740104, 2021.

Plank, S.: Rapid damage assessment by means of multi-temporal SAR- A comprehensive review and outlook to Sentinel-1, Remote Sensing, 6(6), 4870–4906, https://doi.org/10.3390/rs6064870, 2014.

Salman, A., Saha, A., Nomaan, S. S., Haque, E., & Asadi, T.: Assessing Tropical Cyclone Destruction Using Landsat Satellite Imagery: a Case Study in Bangladesh, J. Integr. Disaster Risk Manag., 14(2), https://doi.org/10.5595/001c.123359, 2024.

Tazneen, F., Rahman, H., Rahman, S., Sultana, N., & Faisal, B. R.: Preliminary Application of Space-based Remote Sensing and Geospatial Technology for Investigation on the Geo-environmental Consequences of Cyclone Aila 2009 in Bangladesh, Int. J. Environ. Geoinformat., 8(3), 229–244, https://doi.org/10.30897/ijegeo.837770, 2021.

https://doi.org/10.5194/egusphere-2026-1545
Preprint. Discussion started: 29 April 2026

Torres, R., Snoeij, P., Geudtner, D., Bibby, D., Davidson, M., Attema, E., Potin, P., Rommen, B. Ö., Floury, N., Brown, M., Traver, I. N., Deghaye, P., Duesmann, B., Rosich, B., Miranda, N., Bruno, C., L'Abbate, M., Croci, R., Pietropaolo, A., Huchler, M., and Rostan, F.: GMES Sentinel-1 mission, Remote Sens. Environ., 120, 9–24, https://doi.org/10.1016/j.rse.2011.05.028, 2012.

Touzi, R., Lopes, A., Bruniquel, J., & Vachon, P. W.: Coherence Estimation for SAR Imagery, IEEE Trans. Geosci. Remote Sens., 37(1), 1999.

Tralli, D. M., Blom, R. G., Zlotnicki, V., Donnellan, A., & Evans, D. L.: Satellite remote sensing of earthquake, volcano, flood, landslide and coastal inundation hazards, ISPRS J. Photogramm. Remote Sens., 59(4), 185–198, https://doi.org/10.1016/j.isprsjprs.2005.02.002, 2005.

Uddin, K., & Matin, M. A.: Potential flood hazard zonation and flood shelter suitability mapping for disaster risk mitigation in Bangladesh using geospatial technology, Prog. Disaster Sci., 11, https://doi.org/10.1016/j.pdisas.2021.100185, 2021.

Washaya, P., & Balz, T.: SAR Coherence Change Detection of Urban Areas Affected by Disasters Using Sentinel-1 Imagery, Int. Arch. Photogramm. Remote Sens. Spatial Inf. Sci. - ISPRS Arch., 42(3), 1857–1861, https://doi.org/10.5194/isprs-archives-XLII-3-1857-2018, 2018.

Zebker, H. A., & Villasenor, J.: Decorrelation in Interferometric Radar Echoes, IEEE Trans. Geosci. Remote Sens., 30(5), 1992.